J|A|C|S
ARTICLES
Published on Web 06/02/2007

Luminescent Silica Nanobeads: Characterization and Evaluation as Efficient Cytoplasmatic Transporters for T-Lymphocytes

Massimo Bottini,*,†,‡ Fabio Cerignoli,† David M. Mills,† Federica D'Annibale,‡ Marilisa Leone,† Nicola Rosato,|| Andrea Magrini,‡ Maurizio Pellecchia,† Antonio Bergamaschi,§ and Tomas Mustelin†

Contribution from the Burnham Institute for Medical Research, 10901 North Torrey Pines Road, La Jolla, California 92037, NAST and Department of Environmental, Occupational, and Social Medicine and NAST and Department of Experimental Medicine and Biochemical Sciences, University of Rome Tor Vergata, Via Montpellier 1, 00133 Rome, Italy, and Institute of Occupational Medicine, Università Cattolica del Sacro Cuore, Largo Agostino Gemelli 8, 00168 Rome, Italy

Received January 11, 2007; E-mail: mbottini@burnham.org

Abstract: We report the fabrication and characterization of neutravidin-conjugated silica nanobeads doped with a ruthenium-complex luminophore and functionalized with antihuman CD3, antihuman CD28, and an acid-sensitive polymer. We observed that the nanobeads were readily delivered into Jurkat T leukemia cells by endocytosis, transported into lysosomes and subsequently into the cytoplasm as revealed by pH-sensitive luminescence. Since signs of cytotoxicity were not observed, the reported nanobeads could be an excellent and nontoxic building block for efficient intracellular transporters.

1. Introduction

The emerging field of nanomedicine, the use of the tools and knowledge of nanotechnology for biomedical purposes, is aimed at the preservation and improvement of human health and may lead to the development of more effective means for delivery and targeting of pharmaceutical, therapeutic, and diagnostic agents as compared to current methods.[1] The development of nanotechnology-based agents involves the identification of precise targets (cell type and receptors) related to specific clinical conditions and of an appropriate nanocarrier to achieve the required responses while minimizing side effects. To enhance diagnostic or therapeutic efficacy, novel nanomaterials must have multivalent loading capacity for effective drug delivery, be engineered to function in biologically relevant environments, and facilitate detection. The transport of several types of engineered nanomaterials into adherent and nonadherent mammalian cell lines has been reported.[2−8] Nevertheless, the chemistry of engineered nanomaterials has limited the efficient targeting of a specific cell line and their capacity to interact multivalently with cell membrane receptors. Furthermore, most complexes are internalized by endocytosis and not released into the cytoplasm but rather are trafficked rapidly from endosomes to lysosomes, the organelles that in the general endocytosis pathway enzymatically digest macromolecules and are characterized by a pH of approximately 4.5. The lysosome barrier to cytoplasmic entry represents a significant challenge in the use of nanomaterials as intracellular delivery systems. Recently, pH-sensitive polymers were designed to be inactive at physiological pH and membrane active in the lower pH environment of developing endosomes.[9]

† Burnham Institute for Medical Research.
‡ Department of Environmental, Occupational, and Social Medicine, University of Rome Tor Vergata.
|| INFM and Department of Experimental Medicine and Biochemical Sciences, University of Rome Tor Vergata.
§ Università Cattolica del Sacro Cuore.

(1) (a) Moghimi, S. M.; Hunter, A. C.; Murray, J. C. *FASEB J.* **2005**, *19*, 311. (b) Salata, O. *J. Nanobiotechnology* **2004**, *2*, 3. (c) Wagner, V.; Dullaart, A.; Bock, A. K.; Zweck, A. *Nat. Biotechnol.* **2006**, *24*, 1211.
(2) (a) Slowing, I.; Trewyn, B. G.; Lin, V. S.-H. *J. Am. Chem. Soc.* **2006**, *128*, 14792. (b) Lu, C. W.; Hung, Y.; Hsiao, J. K.; Yao, M.; Chung, T. H.; Lin, Y. S.; Wu, S. H.; Hsu, S. C.; Liu, H. M.; Mou, C. Y.; Yang, C. S.; Huang, D. M.; Chen, Y. C. *Nano Lett.* **2007**, *7*, 149. (c) Kim, J. S.; Yoon, T. J.; Yu, K. N.; Noh, M. S.; Woo, M.; Kim, B. G.; Lee, K. H.; Sohn, B. H.; Park, S. B.; Lee, J. K.; Cho, M. H. *J. Vet. Sci.* **2006**, *7*, 321. (d) Chung, T.-H.; Wu, S.-H.; Yao, M.; Lu, C.-W.; Lin, Y.-S.; Hung, Y.; Mou, C.-Y.; Chen, Y.-C.; Huang, D.-M. *Biomaterials* **2007**, *28*, 2959. (e) Xing, X.; He, X.; Peng, J.; Wang, K.; Tan, W. *J. Nanosci. Nanotechnol.* **2005**, *5*, 1688. (f) Huang, D.-M.; Hung, Y.; Ko, B.-S.; Hsu, S.-C.; Chen, W.-H.; Chien, C.-L.; Tsai, C.-P.; Kuo, C.-T.; Kang, J.-C.; Yang, C.-S.; Mou, C.-Y.; Chen, Y.-C. *FASEB J.* **2005**, *19*, 2014. (g) Lai, C.-Y.; Trewyn, B. G.; Jeftinija, D. M.; Jeftinija, K.; Xu, S.; Jeftinija, S.; Lin, V. S. Y. *J. Am. Chem. Soc.* **2003**, *125*, 4451. (h) Ravi Kumar, M. N.; Sameti, M.; Mohapatra, S. S.; Kong, X.; Lockey, R. F.; Bakowsky, U.; Lindenblatt, G.; Schmidt, H.; Lehr, C. M. *J. Nanosci. Nanotechnol.* **2004**, *4*, 876.
(3) (a) Bottini, M.; Cerignoli, F.; Dawson, M. I.; Magrini, A.; Rosato, N.; Mustelin, T. *Biomacromolecules* **2006**, *7*, 2259. (b) Cai, D.; Mataraza, J. M.; Qin, Z.-H.; Huang, Z.; Huang, J.; Chiles, T. C.; Carnahan, D.; Kempa, K.; Ren, Z. *Nat. Methods* **2005**, *2*, 449. (c) Kostarelos, K.; Lacerda, L.; Pastorin, G.; Wu, W.; Wieckowski, S.; Luangsivilay, J.; Godefroy, S.; Pantarotto, D.; Briand, J.-P.; Muller, S.; Prato, M.; Bianco, A. *Nature Nanotech.* **2007**, *2*, 108.
(4) (a) Shukla, R.; Bansal, V.; Chaudhary, M.; Basu, A.; Bhonde, R. R.; Sastry, M. *Langmuir* **2005**, *21*, 10644.
(5) Panyam, J.; Zhou, W. Z.; Prabha, S.; Sahoo, S. K.; Labhasetwar, V. *FASEB J.* **2002**, *16*, 1217.
(6) (a) Duan, H.; Nie, S. *J. Am. Chem. Soc.* **2007**, *129*, 3333. (b) Delehanty, J. B.; Medintz, I. L.; Pons, T.; Brunel, F. M.; Dawson, P. E.; Mattoussi, H. *Bioconjugate Chem.* **2006**, *17*, 920.
(7) (a) Ito, A.; Shinkai, M.; Honda, H.; Kobayashi, T. *J. Biosci. Bioeng.* **2005**, *100*, 1. (b) Corr, S. A.; O'Byrne, A.; Gun'ko, Y. K.; Ghosh, S.; Brougham, D. F.; Mitchell, S.; Volkov, Y.; Prina-Mello, A. *Chem. Commun.* **2006**, 4474.

 10.1021/ja070245c CCC: $37.00

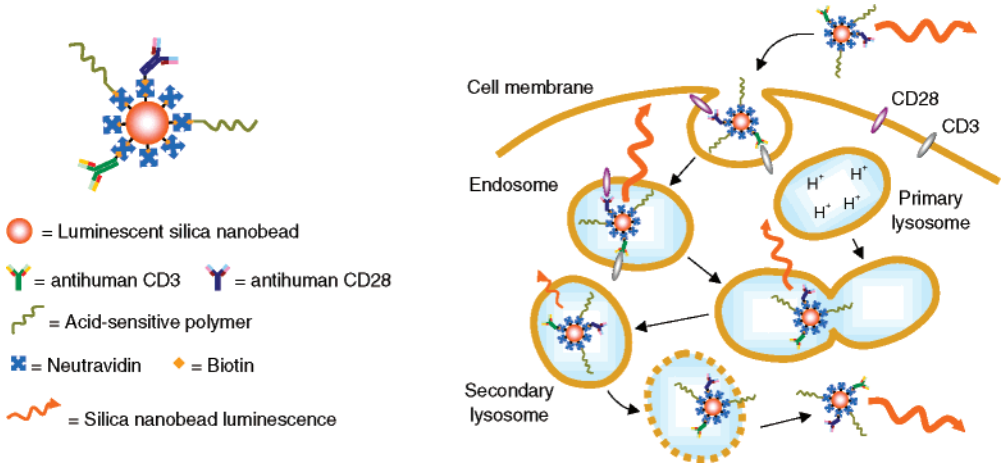

Figure 1. Schematic of neutravidin-conjugated luminescent silica nanobeads functionalized with antibodies for T cell receptor post-signaling endocytosis and an acid-sensitive polymer for disruption of lysosomal compartments. The nanobeads were delivered into Jurkat T leukemia cells through endocytosis, transported into secondary lysosomes through the fusion of endocytotic vescicles with primary lysosomes, and subsequently transported into the cytoplasm as revealed by pH-sensitive luminescence (the extent of which is indicated with orange arrows).

Silica nanobeads (SNB) have been widely used for biosensing and catalytic applications because of their large surface area to volume ratio, straightforward manufacture, and capacity for doping and/or functionalization with fluorescent molecules, magnetic nanobeads, or semiconducting nanocrystals.[2,10−12] The present work focuses on an intracellular transporter constructed from neutravidin-conjugated SNB doped with a ruthenium-complex luminophore and functionalized with antibodies (antihuman CD3 and antihuman CD28) for T cell receptor (TCR) post-signaling endocytosis and an acid-sensitive polymer for disruption of lysosomal compartments (Figure 1). The pH-dependent luminescence of the SNB permitted us to detect by flow cytometry whether the nanobeads were transported across the lysosomal membrane. Furthermore, the nanobeads were hydrophilic, biocompatible, and functionalizable with intracellularly active proteins and nucleic acids by exploiting the strong affinity between biotin and free neutravidin on the SNB surface. Therefore, the reported biomimetic nanoassemblies could be used to achieve a specific cytoplasmic effect in targeted cells.

2. Experimental Procedures

Materials. Unless otherwise noted, reagent-grade chemicals were used without further purification. Deionized water was used for aqueous solutions. Cyclohexane, Triton X-100, *n*-hexanol, tetramethyl orthosilicate (TMOS), (3-aminopropyl)trimethoxysilane (APTS), (3-trihydroxy)silylpropyl methylphosphonate (THPMP), ammonium hydroxide (28% NH_3 in water), chlorotrimethylsilane (CTMS), tris(2,2′-bipyridine)dichlororuthenium(II) hexahydrate ($Ru(bpy)_3$), Annexin V-FITC, propidium iodide, poly-L-lysine, and formaldehyde were from Sigma-Aldrich (St. Louis, MO); amino-terminated poly(2-propylacrylic acid) (PPAA) was from Polymer Source, Inc. (Dorval, Canada); biotinylated antihuman CD3 and antihuman CD28 antibodies were from eBioscience, Inc. (San Diego, CA); normal mouse serum (NMS) was from Santa Cruz Biotechnology (Santa Cruz, CA); normal goat serum (NGS) was from Gibco (Invitrogen Corp., Carlsbad, CA); water-soluble biotin-labeling reagent sulfosuccinimidyl-6-(biotin-amido)hexanoate (sulfo-NHS-LC-biotin), neutravidin (Nav) and Texas Red-conjugated neutravidin (TRNav) were obtained from Pierce Biotechnology, Inc. (Rockford, IL); RPMI-1640 cell culture medium was from Cellgro (Mediatech, Inc., Herndon, VA); fetal bovine serum (FBS) was from Tissue Culture Biologicals (Informagen, Inc., Newington, NH); LysoTracker Green DND-26, FluoReporter biotin quantitation assay kit and FITC-labeled goat antirabbit antibody were obtained from Molecular Probes (Invitrogen Corp., Carlsbad, CA); PBS pH 7.4 (2.7 mM KCl, 1.5 mM KH_2PO_4, 137 mM NaCl and 8.1 mM Na_2HPO_4) was from Mediatech, Inc. (Herndon, VA). Rabbit antihuman CD107A (LAMP-1) antibody was received from Prof. Minoru Fukuda's laboratory (Burnham Institute for Medical Research, La Jolla, CA).[13]

Instrumentation. Sonication and centrifugation were carried out using a Branson 3510 (Branson Ultrasonic Corporation, Danbury, CT) and a Centrifuge 5417R (Eppendorf AG, Hamburg, Germany), respectively. NMR spectra were collected at room temperature on a Bruker Avance-DRX 600-MHz spectrometer equipped with a 5-mm probe and *z*-axis pulsed field gradients. Cell luminescence was assessed using a FACSCanto flow cytometer (channel FL1 for FITC, FL2 for $Ru(bpy)_3$ or PI, and FL5 for Texas Red) and FACSDiva software (BD Biosciences). Confocal microscopy (Radiance 2100/AGR-3Q, BioRad, Hercules, CA) was used to collect luminescent images after excitation at 457 or 488 nm using an argon laser; 60× (1.4-oil immersion) objective was used. Statistical analyses were realized using PRISM 4 for Windows (GraphPad Software, Inc., San Diego, CA).

(8) (a) Dinauer, N.; Balthasar, S.; Weber, C.; Kreuter, J.; Langer, K.; von Briesen, H. *Biomaterials* **2005**, *26*, 5898. (b) Ballthasar, S.; Michaelis, K.; Dinauer, N.; von Briesen, H.; Kreuter, J.; Langer, K. *Biomaterials* **2005**, *26*, 2723.
(9) (a) Murthy, N.; Robichaud, J. R.; Tirrell, D. A.; Stayton, P. S.: Hoffman, A. S. *J. Controlled Release* **1999**, *61*, 137−143. (b) Lackey, C. A.; Press, O. W.; Hoffman, A. S.; Stayton, P. S. *Bioconjugate Chem.* **2002**, *13*, 996.
(10) (a) Tan, W.; Wang, K.; He, X.; Zhao, X. J.; Drake, T.; Wang, L.; Bagwe, R. P. *Med. Res. Rev.* **2004**, *24*, 621. (b) Bagwe, R. P.; Yang, C.; Hilliard, L. R.; Tan, W. *Langmuir* **2004**, *20*, 8336−8342. (c) Bagwe, R. P.; Hilliard, L. R.; Tan, W. *Langmuir* **2006**, *22*, 4357−4362. (d) Santra, S.; Zhang, P.; Wang, K.; Tapec, R.; Tan, W. *Anal. Chem.* **2001**, *73*, 4988. (e) He, X.; Wang, K.; Tan, W.; Li, J.; Yang, X.; Huang, S.; Li, D.; Xiao, D. *J. Nanosci. Nanotechnol.* **2002**, *2*, 317. (f) Tapec, R.; Zhao, X. J.; Tan, W. *J. Nanosci. Nanotechnol.* **2002**, *2*, 405. (g) Yang, H.-H.; Qu, H.-Y.; Lin, P.; Li, S.-H.; Ding, M.-T.; Xu, J.-G. *Analyst* **2003**, *128*, 462. (h) Yang, W.; Zhang, C. G.; Qu, H. Y.; Yang, H. H.; Xu, J. G. *Anal. Chim. Acta* **2004**, *503*, 163. (i) Ye, Z.; Tan, M.; Wang, G.; Yuan, J. *Anal. Chem.* **2004**, *76*, 513. (l) Wang, L.; Yang, C.; Tan, W. *Nano Lett.* **2005**, *5*, 37.
(11) (a) Yi, D. K.; Selvan, S. T.; Lee, S. S.; Papaefthymiou, G. C.; Kundaliya, D.; Ying, J. Y. *J. Am. Chem. Soc.* **2005**, *127*, 4990. (b) Yang, H.-H.; Zhang, S.-Q.; Chen, X.-L.; Zhuang, Z.-X.; Xu, J.-G.; Wang, X.-R. *Anal. Chem.* **2004**, *76*, 1316.
(12) (a) Rogach, A. L.; Nagesha, D.; Ostrander, J. W.; Giersig, M.; Kotov, N. A. *Chem. Mater.* **2000**, *12*, 2676. (b) Gerion, D.; Pinaud, F.; Williams, S. C.; Parak, W. J.; Zanchet, D.; Weiss, S.; Alivisatos, A. P. *J. Phys. Chem. B* **2001**, *105*, 8861. (c) Nann, T.; Mulvaney, P. *Angew. Chem., Int. Ed.* **2004**, *43*, 5393.
(13) Carlsson, S. R.; Roth, J.; Piller, F.; Fukuda, M. *J. Biol. Chem.* **1988**, *263*, 18911.

Preparation of Neutravidin-Conjugated Luminescent Silica Nanobeads. A mixture of cyclohexane, Triton X-100, and *n*-hexanol (volume ratio 4.2:1:1; 24.8-mL final volume) was converted to a nanoemulsion by stirring at room temperature for 1 h before an aqueous solution of $Ru(bpy)_3$ (940 μL) and TMOS (100.5 μL) were added. The final concentration of $Ru(bpy)_3$ in the reaction mixture was 1 mM. This mixture was sonicated for 1 h to facilitate the diffusion of TMOS into the encapsulated water droplets. A drop (59 μL) of 28% aqueous NH_4-OH was added to catalyze the hydrolysis and condensation of TMOS. This mixture was stirred for 24 h before TMOS (10.1 μL) was added, followed 30 min later by a mixture of APTS (6 μL) and THPMP (15.4 μL). After 12 h the hydroxyl groups on the surface of $Ru(bpy)_3$-doped SNB (RuSNB) were capped by the addition of CTMS (8.6 μL) followed by stirring for 12 h. The RuSNB were precipitated with acetone (25 mL). The precipitated RuSNB (approximately 25 mg) were washed several times with water, then with anhydrous ethanol. A 1 mg aliquot of RuSNB and 30 mg of sulfo-NHS-LC-biotin were stirred for 2 h in phosphate-buffered saline (PBS, 2 mL). Nav was kept at 37 °C for 5 min and then centrifuged at 5000g for 5 min to remove protein aggregates. The biotinylated nanobeads (RuSNB−biotin) were washed three times with PBS and then incubated with 5 mg of Nav overnight at room temperature. The Nav−conjugated RuSNB (RuSNB−Nav) were washed with PBS until the absorbance of the wash at 280 nm demonstrated the absence of protein.

We produced control SNB decorated with Nav (SNB−Nav) or TRNav (SNB−TRNav) by following a protocol similar to that for the preparation of RuSNB−Nav by omitting the addition of $Ru(bpy)_3$ during the preparation of the SNB and then incubating the biotinylated control SNB (SNB−biotin) with Nav or TRNav, respectively.

Preparation of Biotinylated Poly(2-propylacrylic acid). PPAA (5 mg) and sulfo-NHS-LC-biotin (1 mg) were dissolved in DMF (50 μL) and PBS (4 mL), respectively. The two solutions were mixed and left to react at room temperature for 2 h. To maximize the yield of biotinylated polymer (PPAA−biotin) another 1 mg of sulfo-NHS-LC-biotin was added and left to react for 2 h. PPAA−biotin was purified from unlinked sulfo-NHS-LC-biotin by dialysis against PBS. The concentration of PPAA−biotin (approximately 1 mg/mL) was determined using a FluoReporter biotin quantitation kit.

Functionalization of Silica Nanobeads with Antibodies and the Acid-Sensitive Polymer. RuSNB−Nav (140 μg, 2.8×10^{-11} mol of RuSNB) in 600 μL of PBS were incubated with 30 μg of an equimolar mixture of antihuman CD3 and antihuman CD28 (10^{-10} moles of each antibody) (RuSNB−Nav-$\alpha_3\alpha_{28}$) for 1 h. Then 50 μL of PPAA−biotin was added (RuSNB−Nav-$\alpha_3\alpha_{28}$p). After 1 h the RuSNB−Nav-$\alpha_3\alpha_{28}$p were washed three times in PBS.

Flow Cytometry. Jurkat T leukemia cells (or Raji lymphoma B cells) were grown in RPMI-1640 supplemented with 10% FBS at 37 °C in 5% CO_2. Cells (10^5) in logarithmic growth were washed with RPMI-1640, resuspended in 270 μL of RPMI-1640, incubated with nanobeads (RuSNB−Nav, RuSNB−Nav-α_3, RuSNB−Nav-$\alpha_3\alpha_{28}$, RuSNB−Nav-$\alpha_3\alpha_{28}$p or SNB−TRNav-$\alpha_3\alpha_{28}$) (7 μg) in PBS (30 μL) at 37 °C in 5% CO_2, washed twice in PBS, and then resuspended in 1.5% formaldehyde in PBS (200 μL).

Cell Toxicity. Jurkat T leukemia cells were grown in RPMI-1640 supplemented with 10% FBS at 37 °C in 5% CO_2. Cells (10^5) in logarithmic growth were washed with RPMI-1640, resuspended in 270 μL of RPMI-1640, and incubated with SNB−Nav-$\alpha_3\alpha_{28}$p (7 μg) in PBS (30 μL) at 37 °C in 5% CO_2. Cells were washed twice with Annexin V (AV) buffer (10 mM HEPES/NaOH, pH 7.4, 140 mM NaCl, 2.5 mM $CaCl_2$), resuspended in a solution of Annexin V-FITC, incubated at 4 °C in the dark for 20 min, washed, resuspended in a solution of propidium iodide (PI), and incubated at 4 °C for 10 min before running the sample on the flow cytometer.

Confocal Microscopy. Jurkat T leukemia cells were grown at 37 °C in 5% CO_2 in RPMI-1640 supplemented with 10% FBS at 37 °C in 5% CO_2 atmosphere. Cells (10^5) in logarithmic growth were washed with RPMI-1640, resuspended in 270 μL of RPMI-1640, incubated with RuSNB−Nav-$\alpha_3\alpha_{28}$ or RuSNB−Nav-$\alpha_3\alpha_{28}$p (7 μg) in PBS (30 μL) at 37 °C in 5% CO_2, and then incubated for 30 min on poly-L-lysine-coated cover slips at 37 °C in 5% CO_2. They were then washed twice in PBS. The cells on the cover slips were fixed for 10 min in 3.7% formaldehyde in PBS, blocked, and permeabilized with PBS containing 5% NMS and 0.3% Triton X-100. To visualize lysosomes, the cells were incubated with rabbit anti-CD107A in PBS containing 3% NMS and 0.1% Triton X-100 and then stained with FITC-labeled goat antirabbit antibody in PBS containing 3% NGS and 0.1% Triton X-100. Alternatively, we visualized the lysosomes using a LysoTracker probe following the protocol of the supplier.

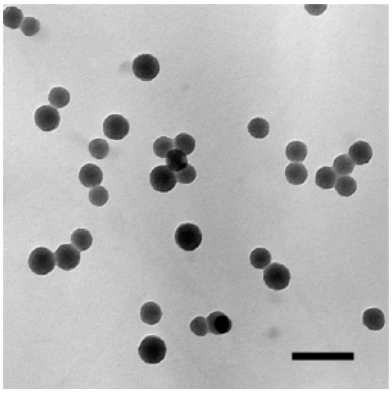

Figure 2. TEM image of luminescent silica nanobeads. Scale bar = 50 nm.

3. Results and Discussion

3.1. Characterization of Luminescent Silica Nanobeads Decorated with Neutravidin. RuSNB were prepared in situ from $Ru(bpy)_3$ using encapsulization in a water-in-oil nanoemulsion. The addition of organosilanes permitted the introduction of phosphonopropyl and 3-aminopropyl groups onto the silica surface. The phosponate groups facilitated the dispersion of RuSNP in PBS and the subsequent biotinylation by coupling the surface amino groups to a biotin-labeling reagent followed by decoration with Nav.

Molecular Weight Estimation of RuSNB. Transmission electron microscope (TEM) images of RuSNB showed uniform diameter (20 ± 1 nm) nanobeads (Figure 2). Assuming that the density of the SNB was equal to pure silica (1.96 g/cm^3) and the weight of encapsulated $Ru(bpy)_3$ was negligible, the weight of one RuSNB having a 20-nm diameter was calculated ($1.96 \times {}^4/_3\pi r^3$) to be approximately 8.2×10^{-18} g and, therefore, the molecular weight of a RuSNB was calculated (weight $\times$ Avogadro number) as approximately 5×10^6.

Loading of Luminophore Molecules in RuSNB and Biotin Groups on RuSNB−Biotin. We recorded the absorbance values at 452 nm of several concentrations of $Ru(bpy)_3$ in PBS to obtain an extinction coefficient $\epsilon_{Rubpy(452\ nm)}$ of approximately 12 500 M^{-1} cm^{-1}. Subsequently, we subtracted the absorbance spectra of SNB dispersed in PBS from that of RuSNB dispersed in PBS to obtain the absorbance spectrum of $Ru(bpy)_3$ encapsulated in RuSNB. From the value of absorbance of encapsulated $Ru(bpy)_3$ at 452 nm and $\epsilon_{Rubpy(452\ nm)}$ we estimated that approximately 300 molecules of $Ru(bpy)_3$ were encapsulated in each RuSNB.

The number of biotin groups on each RuSNB−biotin was determined using the FluoReporter biotin quantitation kit to be approximately 10^4.

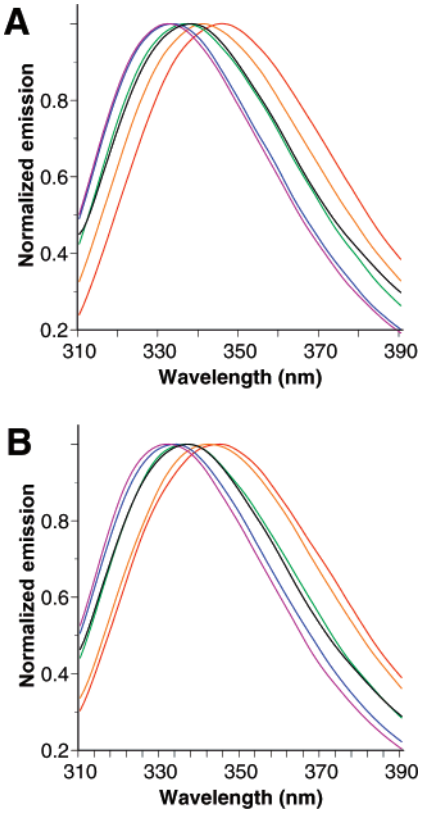

Figure 3. *N*ormalized emission spectra upon excitation at 290 nm for RuSNB−Nav (A) and SNB−TRNav (B) dispersed in PBS (black) and for mixtures in PBS of Nav (A) and TRNav (B) and biotin having molar ratios equal to 1:0 (red), 1:1 (orange), 1:2 (green), 1:3 (blue), and 1:4 (magenta).

Table 1. Maximum Emission Wavelength and Full-Width Half-Maximum, for RuSNB−Nav Dispersed in PBS and for Mixtures with Different Molar Ratios of Nav to Biotin in PBS

sample	λ_{max}[a] (nm)	fwhm[b] (nm)
RuSNB−Nav	338	61
Nav/biotin = 1:0	346	63
Nav/biotin = 1:1	341	61
Nav/biotin = 1:2	337	59
Nav/biotin = 1:3	333	56
Nav/biotin = 1:4	332	55

[a] Maximum emission wavelength. [b] Full-width half-maximum.

Loading of Nav on RuSNB−Nav. The presence of linked Nav on the surface of RuSNB−Nav was determined on the basis of the following observation. It has been reported that biotin binding blue-shifts the tryptophan luminescence emission peak (λ_{max}) and reduces the bandwidth at half-height (full-width half-maximum, fwhm).[14] Streptavidin and Nav are both tetrameric proteins carrying three tryptophans in each monomer. Upon excitation at 290 nm the RuSNB−Nav dispersion in PBS showed an emission band that was blue-shifted and narrower than that exhibited by free Nav dispersed in PBS (Figure 3A and Table 1). We prepared mixtures having molar ratios between Nav and biotin from 1:1 to 1:4. After 2 h of incubation we collected their emission spectra after excitation at 290 nm. The tryptophan luminescence emission peak was observed to blue-shift and narrow with increasing biotin. In particular in the case of Nav/biotin molar ratio equal to 1:2 the emission spectrum resembled the one exhibited by RuSNB−Nav. Similar results

(14) Kurzban, G. P.; Gitlin, G.; Bayer, E. A.; Wilchek, M.; Horowitz, P. M. *J. Protein Chem.* **1990**, *9*, 673.

Table 2. Maximum Emission Wavelength and Full-Width Half-Maximum, for SNB−TRNav Dispersed in PBS and for Mixtures with Different Molar Ratios of TRNav to Biotin in PBS

sample	λ_{max}[a] (nm)	fwhm[b] (nm)
SNB−TRNav	337	60
TRNav/biotin = 1:0	345	65
TRNav/biotin = 1:1	342	64
TRNav/biotin = 1:2	336	60
TRNav/biotin = 1:3	334	57
TRNav/biotin = 1:4	332	56

[a] Maximum emission wavelength. [b] Full-width half-maximum.

were obtained with SNB−TRNav and free TRNav dispersed in PBS (Figure 3B and Table 2). The latter results suggest that each Nav (or TRNav) was linked to RuSNB−biotin (or SNB−biotin) through approximately two biotin molecules.

We recorded the absorbance values at 283 nm of several concentrations of Nav in PBS to obtain an extinction coefficient $\epsilon_{Nav(283\ nm)}$ of approximately $1.1 \times 10^5\ M^{-1}\ cm^{-1}$. We subtracted the absorbance spectrum of RuSNB in PBS from the spectrum of RuSNB−Nav to obtain the spectrum of Nav linked to RuSNB. From the value of absorbance of Nav linked to RuSNB at 283 nm and $\epsilon_{Nav(283\ nm)}$ we calculated that approximately 40 proteins were on each RuSNB−Nav. A similar value was calculated for the number of TRNav on each SNB−TRNav.

Spectroscopic Properties of RuSNB−Nav. Samples (500 μL) used for NMR spectroscopy consisted of free Ru(bpy)$_3$ (100 μM) and RuSNB−Nav (at a concentration such that encapsulated Ru(bpy)$_3$ had a concentration of 100 μM) in PBS at pH 7.4 containing 10% D_2O. The pH was changed by successive additions of concentrated HCl. ^{1}H NMR spectra were acquired with 4096 data points, 1024 scans, and a relaxation delay of 1 s; a 90° pulse of 7 μs was implemented. Water suppression was achieved by means of a WATERGATE pulse scheme. The NMR spectrum of Ru(bpy)$_3$ at pH 7.4 (Figure 4A, black curve) exhibited sharp signals from the bipyridyl protons. Encapsulation of Ru(bpy)$_3$ into the silica network caused large broadening of all NMR resonances although no shift in the signal positions with respect to the free chelate in solution was detected (Figure 4B, black curve). This result suggests a strong electrostatic interaction between Ru(bpy)$_3$ and the silica surface, which is negatively charged at physiological pH, that would decrease the total correlation time of the molecule and a rapid transverse relaxation that is generally characteristic of large macromolecular structures.

The absorbance spectra of both free and encapsulated Ru(bpy)$_3$ dissolved in PBS at pH 7.4 were characterized by a narrow peak at approximately 290 nm and a broad plateau in the 400−480 nm range, which we attribute to a ligand-to-ligand $\pi \rightarrow \pi^*$ transition and a d $\rightarrow \pi^*$ metal-to-ligand charge-transfer transition, respectively. The peaks in the spectrum of the encapsulated Ru(bpy)$_3$ in PBS were slightly red-shifted and broader compared to those of free Ru(bpy)$_3$ (Figure 5A). In steady-state experiments, excitation of RuSNB−Nav in PBS at 452 nm produced an emission band that was enhanced, blue-shifted, and slightly narrower compared to that of free Ru(bpy)$_3$ in PBS (Figure 5B). The emission spectra were collected after having matched absorptions at the 452 nm excitation wavelength of free and encapsulated Ru(bpy)$_3$. These results suggest that after encapsulation into the silica network the luminophore underwent a change in the conformation and a decrease in

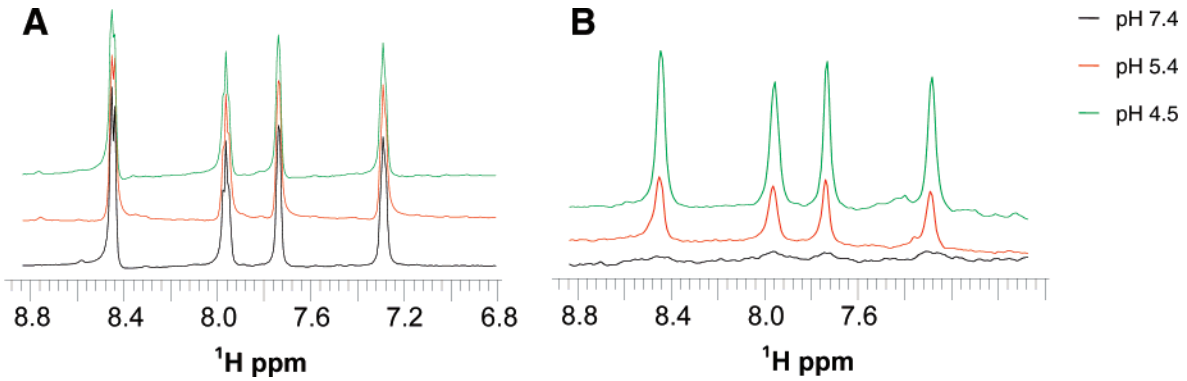

Figure 4. NMR spectrum of free $Ru(bpy)_3$ (A) and RuSNB−Nav (B) in PBS at different pH values containing 10% D_2O.

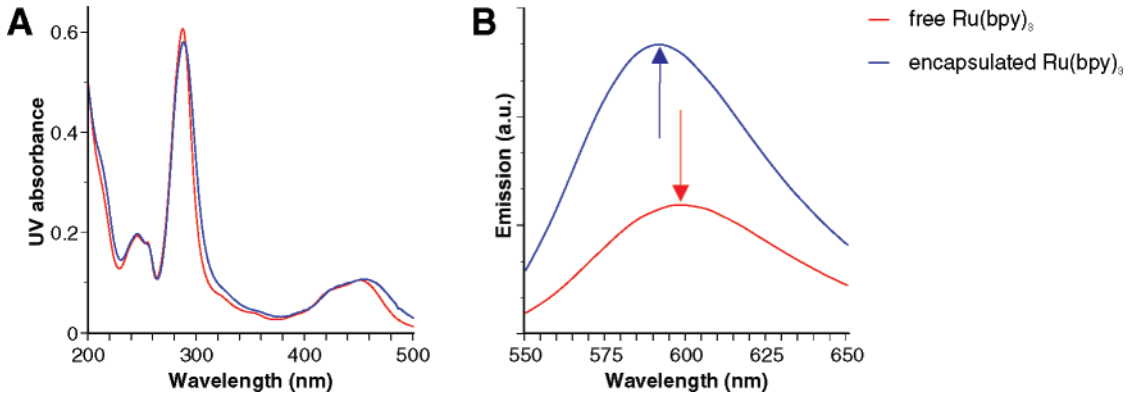

Figure 5. (A) Absorbance spectra of free and encapsulated $Ru(bpy)_3$ in PBS at pH 7.4. The absorbance spectrum of encapsulated $Ru(bpy)_3$ was obtained by subtracting from the spectrum of RuSNB−Nav those of both SNB and Nav in PBS. (B) Emission spectra upon excitation at 452 nm of free and encapsulated $Ru(bpy)_3$ in PBS at pH 7.4. Emission spectra were recorded after matching the absorbance values at 452 nm for free and encapsulated $Ru(bpy)_3$. Arrows indicate the emission peaks of encapsulated (blue arrow) and free (red arrow) $Ru(bpy)_3$ in PBS at pH 7.4.

mobility owing to strong electrostatic interactions with the silica surface. The increase in intensity of the emission peak can be accounted for by the decrease in mobility. It has been reported that luminophore mobility facilitates rapid internal conversion and efficient relaxation of the excited-state via nonradiative pathways because of intersections of the ground and excited-state energy surfaces.[15,16] The blue-shift and the decrease of full-width half-maximum of the emission peak can be accounted for by solvent-$Ru(bpy)_3$ interactions. As previously reported, the solvent reorganization energy term (χ) may influence the excited-state decay of luminophores in aqueous medium and changes in χ may affect the emission band line width.[17−19] The silica surface of the nanobead pores contains a regularly spaced pattern of oxygen atoms that could serve as hydrogen-bond acceptors, promote ordered water structure, and vary the solvation sphere of the encapsulated luminophores, thereby explaining the observed changes in line width.The effects of changing solvent polarity[20,21] and pH[22,23] on the photophysical properties of many homo- and heteroleptic complexes of Ru(II) and Ru(II) complex-modified amino acids have been widely investigated. In particular, it has been reported that protonation of the metal-to-ligand charge-transfer excited states leads to a diminution of luminescence lifetime and intensity. We analyzed the photophysical properties of free $Ru(bpy)_3$ and RuSNB−Nav in PBS at pHs ranging from the physiologic value of 7.4 to 4. The NMR (Figure 4A), absorbance (data not shown), and emission (data not shown) spectra of free $Ru(bpy)_3$ in PBS were not influenced by changes in pH. Indeed, because $Ru(bpy)_3$ does not have a basic nitrogen on its periphery, its ground and excited states are not capable of being protonated. The NMR line broadening of RuSNB−Nav was strongly and gradually attenuated with decreasing pH (Figure 4B). The absorbance spectrum of SNB−Nav increased with increases in pH (Figure 6A) probably as a consequence of an increase in the extinction coefficient of the silica network due to its protonation. The absorbance spectrum of RuSNB−Nav exhibited the following features as the pH decreased: (i) background increases as was observed for SNB−Nav; (ii) decrease in intensity of the narrow peak at approximately 290 nm (Figure 6B); (iii) decrease in intensity of the broad plateau in the 400−480 nm range with the two peaks being slightly blue-shifted and changing their relative intensity (Figure 6C). Upon excitation at 452 nm, the

Table 3. Maximum Emission Wavelength and Full-Width Half-maximum for Free $Ru(bpy)_3$ and RuSNB−Nav in PBS at pH 7.4

sample	λ_{max}[a] (nm)	fwhm[b] (nm)
$Ru(bpy)_3$	598	72
RuSNB−Nav	591	70

[a] Maximum emission wavelength. [b] Full-width half-maximum.

(15) Webber, N. M.; Litvinenko, K. L.; Meech, S. R. *J. Phys. Chem. B* **2001**, *105*, 8036.
(16) Kummer, A. D.; Kompa, C.; Niwa, H.; Hirano, T.; Kojima, S.; Michel-Beyerle, M. E. *J. Phys. Chem. B* **2002**, *106*, 7554.
(17) Cha, X.; Ariga, K.; Kunitake, T. *J. Am. Chem. Soc.* **1996**, *118*, 9545.
(18) Caspar, J. V.; Meyer, T. J. *J. Am. Chem. Soc.* **1983**, *105*, 5583.
(19) Caspar, J. V.; Sullivan, B. P.; Kober, E. M.; Meyer, T. J. *Chem. Phys. Lett.* **1982**, *91*, 91.
(20) Sun, H.; Hoffman, M. Z. *J. Phys. Chem.* **1993**, *97*, 11956.
(21) Nair, R. B.; Cullum, B. M.; Murphy, C. J. *Inorg. Chem.* **1997**, *36*, 962.
(22) Sun, H.; Hoffman, M. Z. *J. Phys. Chem.* **1993**, *97*, 5014−5018.
(23) Cargill Thompson, A. M. W.; Smailes, M. C. C.; Jeffery, J. C.; Ward, M. D. *J. Chem. Soc., Dalton Trans.* **1997**, 737−743.

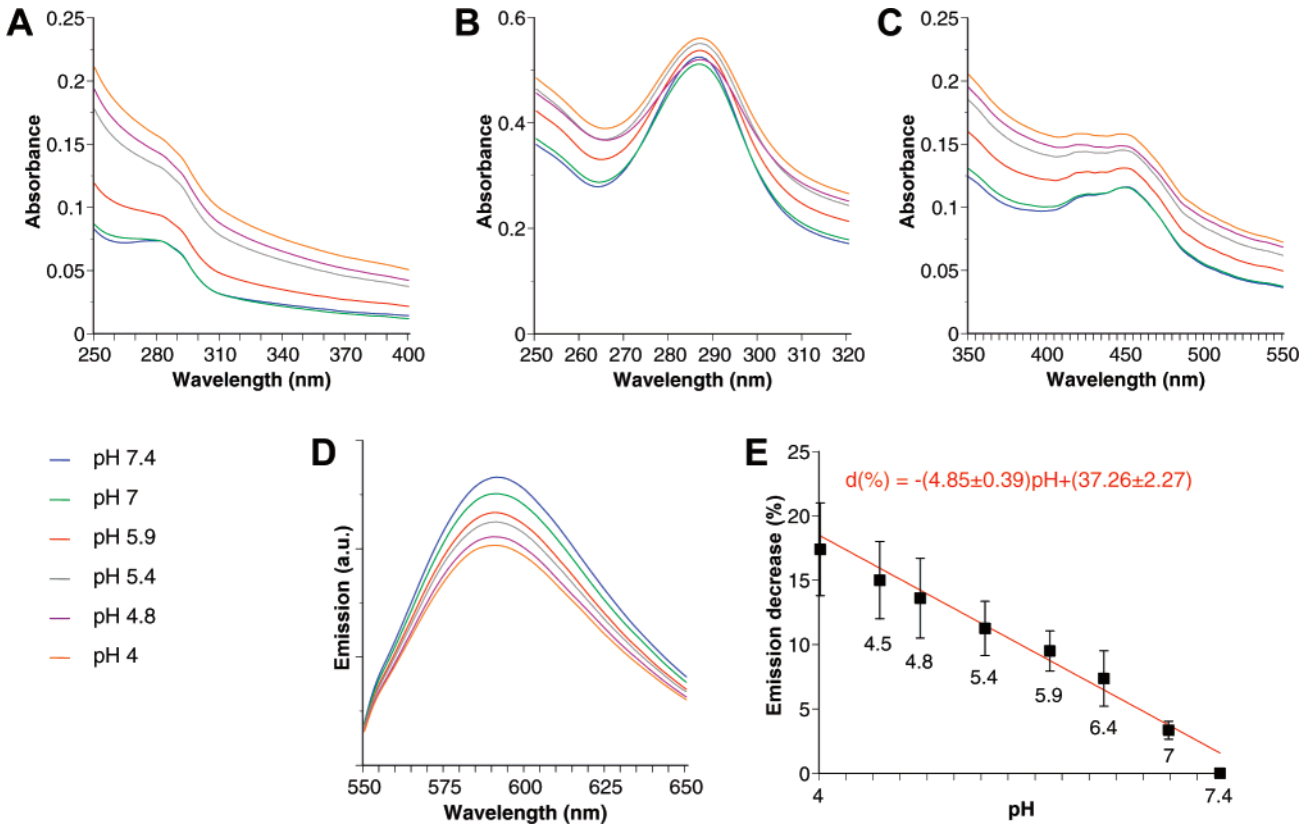

Figure 6. (A) Absorbance spectra of SNB−Nav dispersed in PBS at pH values of 4 to 7.4; (B) absorbance spectra in the UV range (corresponding to the ligand-to-ligand $\pi \rightarrow \pi^*$ transition) and (C) in the visible range (corresponding to the d $\rightarrow \pi^*$ metal-to-ligand charge-transfer transition) of RuSNB−Nav dispersed in PBS at pH values of 4 to 7.4; (D) emission spectra of RuSNB−Nav dispersed in PBS at pH values of 4 to 7.4. The absorbance and emission spectra were corrected by the corresponding concentration factors. (E) Decrease of RuSNB−Nav emission intensity with changing the pH. Errors bars represent the standard deviations for triplicate experiments.

emission peak at 591 nm linearly decreased in intensity (Figure 6D and E) without any significant change in the line width. The observed changes in photophysical properties of encapsulated $Ru(bpy)_3$ could be explained by silica network protonation that reduced the strength of the electrostatic interactions between the metal complex and the matrix and, therefore, increased mobility of the encapsulated luminophore. Higher mobility leads to an increase of the number of collisional encounters between the luminophore and the protonated silica network to quench luminescence while changes in the solvation sphere of encapsulated $Ru(bpy)_3$ are unlikely to explain the observed pH-dependent luminescence quenching because no significant changes in the line width were observed.

3.2. Cell Internalization of Luminescent Silica Nanobeads Decorated with Neutravidin. We first determined the maximum number of antibodies that linked each RuSNB−Nav. RuSNB−Nav (4 μg, approximately 8×10^{-13} mol of RuSNB, assuming a molecular weight of 5×10^6, decorated with approximately 3.2×10^{-11} moles of Nav, assuming 40 proteins on each RuSNB−Nav) in 20 μL of PBS were incubated with 6 μg of an equimolar mixture of antihuman CD3 and antihuman CD28 (2×10^{-11} moles of each antibody, assuming a molecular weight of 1.5×10^5) for 1 h. The nanobeads were washed three times with PBS by centrifugation to give RuSNB−Nav-$\alpha_3\alpha_{28}$. We estimated the amount of antibody that bound the RuSNB−Nav by using polyacrylamide gel electrophoresis and Western immunoblotting. We observed that approximately 2.5−3.0 μg ($(1.6-2) \times 10^{-11}$ mol) of total antibody was linked to the RuSNB−Nav while most the remaining 3.0−3.5 μg of total

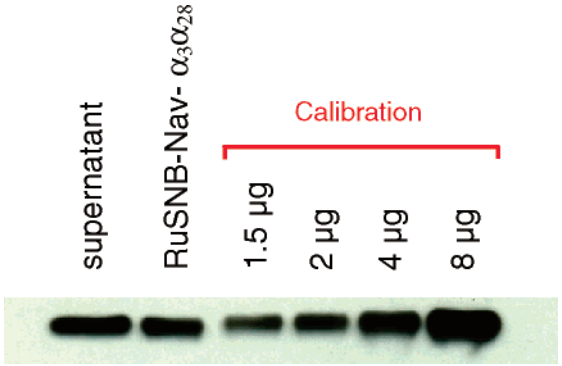

Figure 7. Western blot analysis of the antibodies (antihuman CD3 and antihuman CD28) linked to 4 μg of RuSNB−Nav. RuSNB−Nav were incubated with 6 μg of an equimolar mixture of antihuman CD3 and antihuman CD28 for 1 h, then washed with centrifugation three times with PBS. Lanes 1 and 2 were the superrnatant fraction collected after the first wash and the pellet (RuSNB−Nav-$\alpha_3\alpha_{28}$) collected after the third wash, respectively. The other lanes contained different levels of equimolar antihuman CD3 and antihuman CD28 to obtain a loading curve.

antibody was in the supernatant fraction collected after the first wash (Figure 7). This result suggests that the maximum number of antibodies that can be linked to a single RuSNB−Nav was between 20 and 25, which corresponds to approximately half of the Nav decorating the surface of the nanoparticle.

For cell internalization experiments RuSNB−Nav (140 μg, 2.8×10^{-11} mol of RuSNB) were incubated with 30 μg of an equimolar mixture of antihuman CD3 and antihuman CD28 (10^{-10} moles of each antibody). We verified the level of antibodies linked to the RuSNB−Nav using polyacrylamide gel

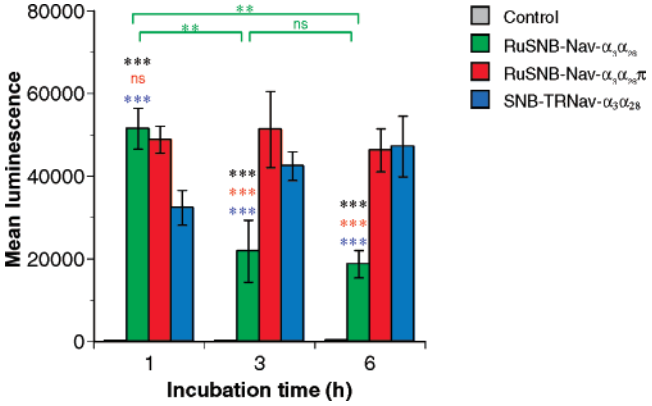

Figure 8. Luminescence-intensity dependence on the incubation time of Jurkat T leukemia cells with RuSNB−Nav-$\alpha_3\alpha_{28}$, RuSNB−Nav-$\alpha_3\alpha_{28}$p, or SNB−TRNav-$\alpha_3\alpha_{28}$. Nontreated cells were used as control (gray). Statistical analysis consisted of a one-way analysis of variance (with Bonferroni's multiple comparison test) for RuSNB−Nav-$\alpha_3\alpha_{28}$ (green) and two-way ANOVA (with Bonferroni's post-test) for RuSNB−Nav-$\alpha_3\alpha_{28}$ vs control (black), RuSNB−Nav-$\alpha_3\alpha_{28}$p (red), and SNB−TRNav-$\alpha_3\alpha_{28}$ (blue): ns = $P > 0.05$; * = $P < 0.05$; ** = $P < 0.01$; *** = $P < 0.001$. Errors bars represent the standard deviation for triplicate experiments.

electrophoresis and Western immunoblotting. The fact that the supernatant fraction collected after the first wash did not contain free antibodies suggested that all antibodies were linked to the Nav on the RuSNB−Nav and, therefore, that approximately seven antibodies were available for each RuSNB−Nav-$\alpha_3\alpha_{28}$ (and RuSNB−Nav-$\alpha_3\alpha_{28}$p).

RuSNB−Nav-$\alpha_3\alpha_{28}$ were readily internalized into Jurkat cells. The internal luminescence of cells treated with RuSNB−Nav-$\alpha_3\alpha_{28}$ was observed to significantly decrease within the first 3 h of incubation suggesting that in the first hours of incubation, RuSNB−Nav-$\alpha_3\alpha_{28}$ were continuously endocytosed by the cells, trafficked into the endosomes, and then transported rapidly to the lysosomes where their luminescence was quenched (Figure 8 and Supporting Information (SI)). As a control, we treated Jurkat cells with SNB decorated with Texas Red-conjugated Nav (SNB−TRNav), which were subsequently functionalized with antihuman CD3 and antihuman CD28 (SNB−TRNav-$\alpha_3\alpha_{28}$). We observed a slight increase in cell luminescence over time (Figure 8 and SI), which was probably due to the continuous cellular uptake of nanobeads since SNB−TRNav dispersed in PBS did not show any variation in emission intensity with decreasing pH.

The data suggest that binding of nanobeads to CD3 and CD28 was able to induce signaling through the TCR, and that signaling-induced endocytosis led to internalization of the antibody-covered nanobeads. TCR signaling induced by crosslinked antihuman CD3 with or without antihuman CD28 is followed by receptor internalization, which is a mechanism of signaling down regulation ("post-signaling endocytosis"). Microbeads are currently used as cross-linkers to induce TCR signaling. Our data suggest that nanobeads work as crosslinkers as well. Indeed T cells incubated for 1 h with RuSNB−Nav-α_3 or with RuSNB−Nav-$\alpha_3\alpha_{28}$ showed increased expression of CD69 (a marker of T cell activation) when compared to cells incubated with RuSNB−Nav (data not shown). Increased signaling following CD28 co-stimulation led to proportionally increased uptake of nanobeads through post-signaling endocytosis. Indeed lower uptake for antihuman CD3-conjugated RuSNB−Nav (RuSNB−Nav-α_3) was observed to suggest that the co-stimulation of both CD3 and CD28 membrane receptors by RuSNB−Nav-$\alpha_3\alpha_{28}$ increased the efficiency of the T cell receptor post-signaling endocytotic internalization (Figure 9). Internalization of nonconjugated RuSNB−Nav by Jurkat cells and of RuSNB−Nav-$\alpha_3\alpha_{28}$ by Raji lymphoma B cells was very weak, suggesting that without stimulation of membrane receptors or in the absence of specific surface receptors endocytotic uptake of RuSNB−Nav was probably only due to nonspecific interactions between the nanobeads and hydrophobic regions of the cell surface (Figure 9).

We next investigated the possibility of lysosomal release of RuSNB−Nav by measuring variations in internal cell luminescence. RuSNB−Nav-$\alpha_3\alpha_{28}$ were functionalized with a pH-sensitive α-propyl acrylic acid polymer (RuSNB−Nav-$\alpha_3\alpha_{28}$p). Jurkat T cells readily internalized RuSNB−Nav-$\alpha_3\alpha_{28}$p and exhibited an internal luminescence that was time-independent, not statistically significant different from that of cells treated with RuSNB−Nav-$\alpha_3\alpha_{28}$ after 1 h of incubation and higher than that of cells treated with RuSNB−Nav-$\alpha_3\alpha_{28}$ after 3 and 6 h of incubation (Figure 8 and SI). These results suggest that the polymer did not inhibit T cell receptor post-signaling endocytosis and enabled the release of the RuSNB−Nav-$\alpha_3\alpha_{28}$p from the lysosomes as soon as the nanobeads were transported into them.

Intracellular trafficking of RuSNB−Nav-$\alpha_3\alpha_{28}$ and RuSNB−Nav-$\alpha_3\alpha_{28}$p was investigated by confocal microscopy (Figure 10). RuSNB−Nav-$\alpha_3\alpha_{28}$ were readily internalized by cells and transported into lysosomal compartments (Figure 10, panels a, b, and c) as shown by the yellow luminescence (images C and D) corresponding to colocalization of lysosomes (green, image

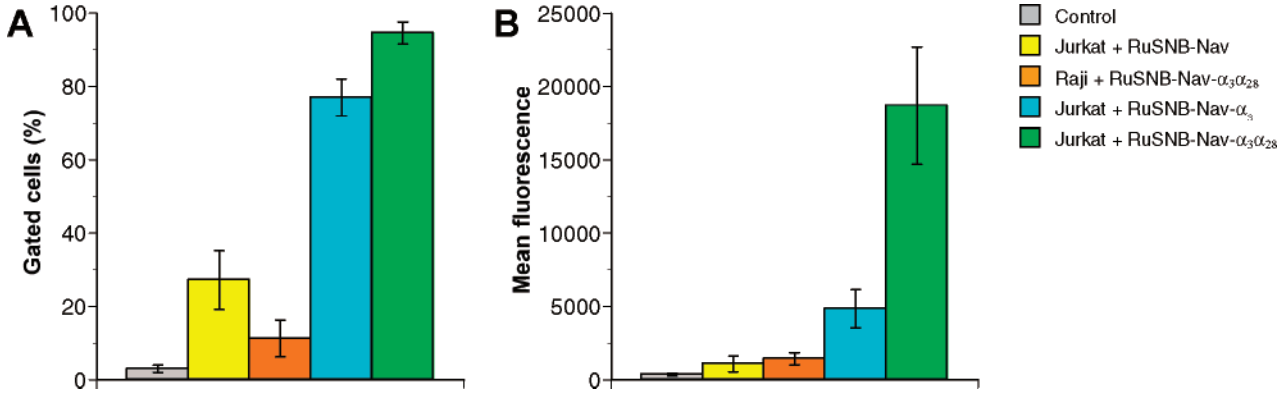

Figure 9. Efficiency (A) and luminescence intensity (B) of Jurkat T leukemia cells incubated for 6 h with RuSNB−Nav, RuSNB−Nav-α_3 and RuSNB−Nav-$\alpha_3\alpha_{28}$ and of Raji lymphoma B cells incubated for 6 h with RuSNB−Nav-$\alpha_3\alpha_{28}$. Nontreated cells were used as control. Errors bars represent the standard deviation for triplicate experiments.

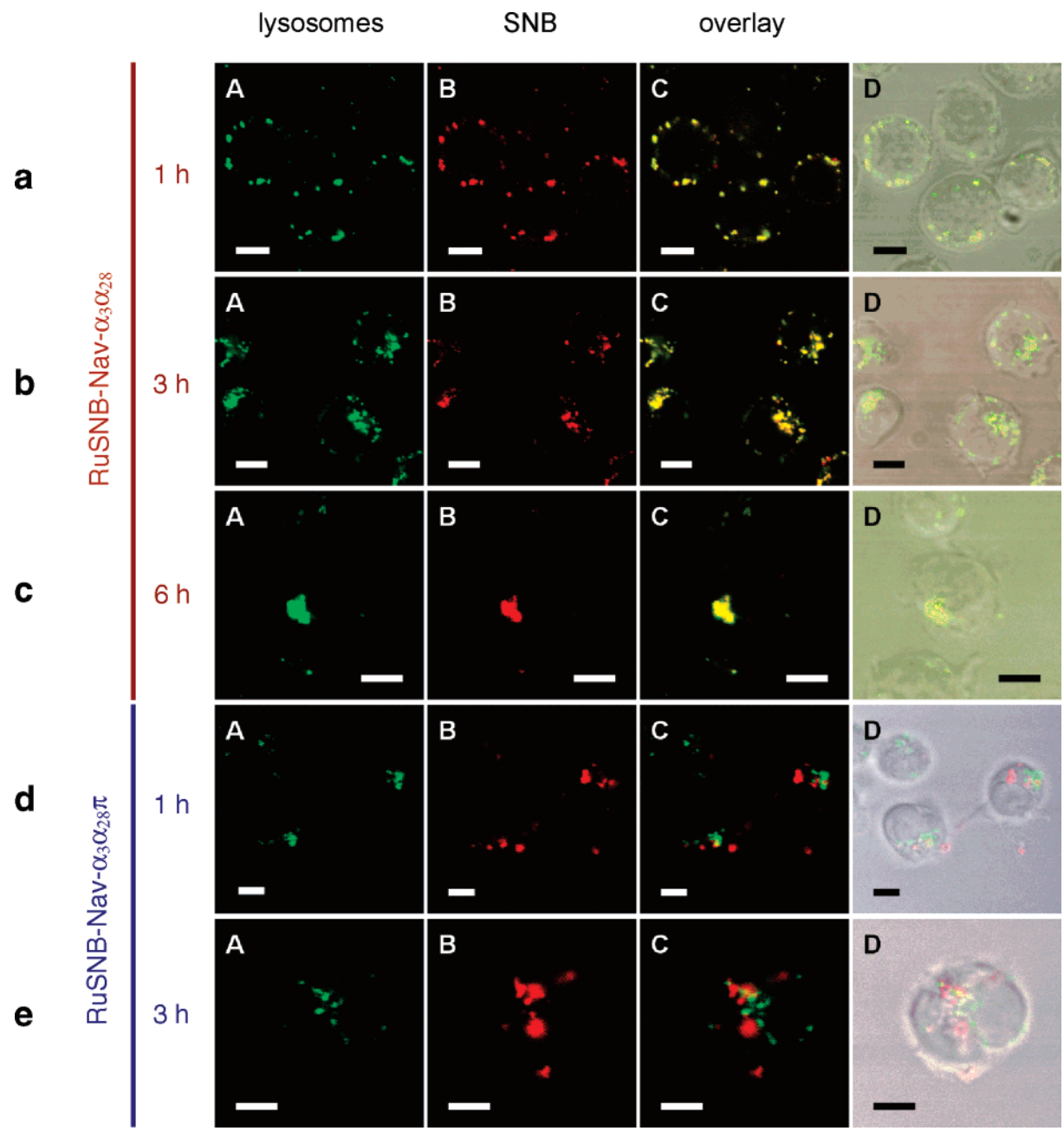

Figure 10. Confocal images of Jurkat T leukemia cells incubated with RuSNB−Nav-$\alpha_3\alpha_{28}$ for 1 (panel a), 3 (panel b), and 6 (panel c) h and with RuSNB−Nav-$\alpha_3\alpha_{28}$p for 1 (panel d) and 3 (panel e) h. Images A and B showed lysosomal compartments and nanobeads, respectively. Image C is the superposition of A and B. Image D is the superposition of C and the bright-field image of the cells. The cells were incubated with rabbit anti-CD107A and then with FITC-labeled goat antirabbit antibody in order to visualize lysosomes. Scale bars are approximately 2.5 μm.

A) and intracellular nanobeads (red, image B). The luminescent features exhibited morphological changes with increasing incubation time. In particular, after 1 h incubation the cells mainly exhibited peripheral punctuate features (panel a). After 3 h of incubation less peripheral features were observed while more internal punctuate features appeared (panel b). After 6 h of incubation cells exhibited only a few intense luminescent features intracellularly. These results confirm the result obtained by flow cytometry that cells continuously internalized nanobeads primarily during the first 3 h of incubation. The peripheral features most likely correspond to endocytosed nanobeads just delivered into lysosomal compartments and, therefore, close to the cell membrane. Subsequently, the lysosomes encapsulating the nanobeads were trafficked intracellularly and finally fused to form a few large vescicles as revealed by their intense luminescent features after 6 h of incubation.

RuSNB−Nav-$\alpha_3\alpha_{28}$p were released from the lysosomes even after only 1 h of incubation (Figure 10, panel d) suggesting that the polymer disrupted the lysosomal compartments as soon as the nanobeads were transported into them. After 3 h of incubation, nanobeads released from lysosomes were localized in a more internal part of the cell (Figure 10, panel e).

In the previous confocal evaluations lysosomes were visualized using an antibody specific for endosomal/lysosomal compartments (rabbit anti-CD107A)[13] after having fixed and permeabilized the cells. Permeabilization of endosomal/lysosomal membranes could lead to leakage of the nanobeads from the vescicles and, therefore, compete with the acid-sensitive

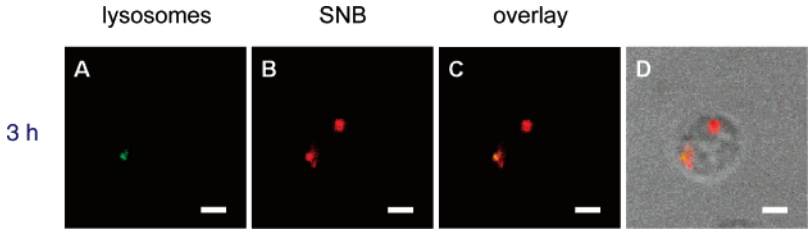

Figure 11. Confocal images of Jurkat T leukemia cells incubated with RuSNB−Nav-$\alpha_3\alpha_{28}$p for 3 h and treated with LysoTracker to stain lysosomal compartments to avoid any membrane permeabilization. Images A and B showed lysosomal compartments and nanobeads, respectively. Image C is the superposition of A and B. Image D is the superposition of C and the bright-field image of the cells. Scale bars are approximately 2.5 μm.

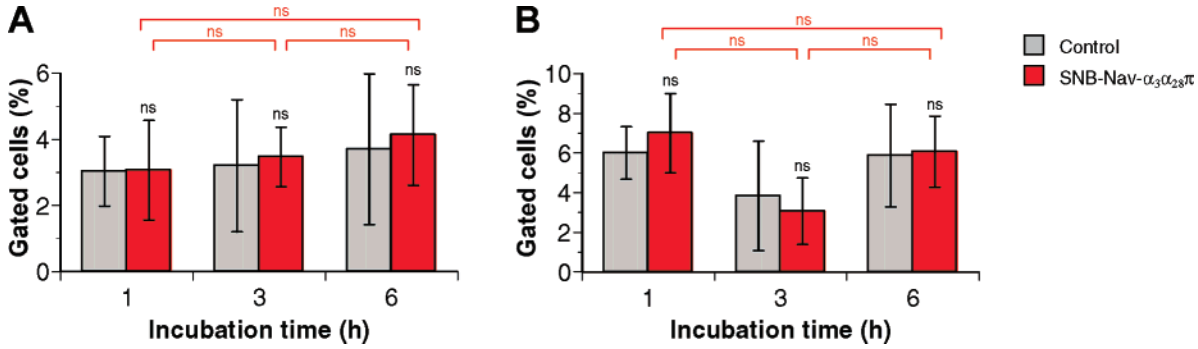

Figure 12. Percentage of apoptotic (A) and necrotic (B) Jurkat leukemia T cells 1, 3, and 6 h after incubation with SNB−Nav-$\alpha_3\alpha_{28}$p (red) and treatment with Annexin V-FITC and PI to visualize apoptotic and necrotic cells, respectively. Nontreated cells were used as a control (gray). Statistical analysis is a one-way analysis of variance (with Bonferroni's multiple comparison test) for SNB−Nav-$\alpha_3\alpha_{28}$p (red) and two-way ANOVA (with Bonferroni's post-test) for SNB−Nav-$\alpha_3\alpha_{28}$p vs control (black): ns = $P > 0.05$. Errors bars represent the standard deviation for triplicate experiments.

polymer. To confirm that the observed cytoplasmatic nanobeads were the result of the action of the polymer, we visualized the lysosomes using LysoTracker that was conjugated with a green luminophore which allowed us to perform the investigation without any previous membrane permeabilization. As showed in Figure 11, after 3 h of incubation with RuSNB−Nav-$\alpha_3\alpha_{28}$p, the red luminescence of the nanobeads overlapped only partially with the green luminescence of lysosomes thereby confirming that the previously observed cytoplasmatic nanobeads were the result of the disruption of the lysosomal compartments by the acid-sensitive polymer and not due to internal leakage resulting from membrane permeabilization.

Cells incubated with RuSNB−Nav-$\alpha_3\alpha_{28}$p showed intrinsic punctuate cytoplasmatic luminescence throughout the incubation time and independently of the technique used to visualize the lysosomes (Figure 10, panels d and e, and Figure 11). Punctuate (rather than diffuse) cytosolic luminescent features corresponding to nanoparticles that had escaped from lysosomes have been reported[2a,6a] and could be explained by a partial aggregation of nanoparticles during their permanence in the vesicles or, more likely, after their release into cytosol. However, the cause of this phenomenon is not clear at the moment and further investigation is warranted to understand the effect of surface functionality on cytoplasmic nanobead aggregation.

The reported results suggest that our nanobeads could be useful to achieve a specific cytoplasmatic effect in targeted cells. However, before developing any therapeutic applications, in vitro and in vivo, short- and long-term cytotoxic effects must be accurately established. Indeed, many nanomaterials (carbon nanotubes,[25] fullerenes,[26] quantum dots,[27] gold nanobeads,[28] etc.) have shown signs of toxicity dependent upon such factors as dose, dimension, chemical functionalization, and physical aspect. Flow cytometry data showed that treatment with SNB−Nav-$\alpha_3\alpha_{28}$p did not induce any toxic effects on Jurkat T cells as compared to nontreated cells. Indeed, the number of apoptotic (AV^+) and necrotic (PI^+) cells was not significantly changed 1, 3, and 6 h after treatment with RuSNB−Nav-$\alpha_3\alpha_{28}$p and was not statistically different with respect to that of nontreated cells (control) (Figure 12 and SI).

Conclusions

In this article we report the fabrication and characterization of silica nanobeads doped with $Ru(bpy)_3$, characterized by pH-dependent luminescence and functionalized with antihuman CD3 and antihuman CD28, and with an acid-sensitive polymer. These nanoparticles were efficiently delivered into Jurkat T cells through T cell receptor post-signaling endocytosis, transported into lysosomal compartments, and subsequently transported to the cytoplasmatic region. Since signs of cytotoxicity were not observed, the reported nanobeads could be an excellent and nontoxic building block for efficient intracellular transporters.

Acknowledgment. This work was supported by Grant U54 CA119335-02 from the National Institutes of Health and by PRIN Grant No. 2006069554 from the Italian Ministry of

(24) Alcover, A.; Alarcon, B. *Crit. Rev. Immunol.* **2000**, *20*, 325.

(25) Bottini, M.; Bruckner, S.; Nika, K.; Bottini, N.; Bellucci, S.; Magrini, A.; Bergamaschi, A.; Mustelin, T. *Toxicol. Lett.* **2006**, *160*, 121. (b) Sayes, C. M.; Liang, F.; Hudson, J. L.; Mendez, J.; Guo, W.; Beach, J. M.; Moore, V. C.; Doyle, C. D.; West, J. L.; Billups, W. E.; Ausman, K. D.; Colvin, V. L. *Toxicol. Lett.* **2006**, *161*, 135. (c) Cui, D.; Tian, F.; Ozkan, C. S.; Wang, M.; Gao, H. *Toxicol. Lett.* **2005**, *155*, 73. (d) Fiorito, S.; Serafino, A.; Andreola, F.; Togna, A.; Togna, G. *J. Nanosci. Nanotechnol.* **2006**, *6*, 591.

(26) Sayes, C. M.; Gobin, A. M.; Ausman, K. D.; Mendez, J.; West, J. L.; Colvin, V. L. *Biomaterials* **2005**, *26*, 7587.

(27) (a) Chang, E.; Thekkek, N.; Yu, W. W.; Colvin, V. L.; Drezek, R. *Small* **2006**, *2*, 1412. (b) Chan, W. H.; Shiao, N. H.; Lu, P. Z. *Toxicol. Lett.* **2006**, *167*, 191. (c) Lovric, J.; Bazzi, H. S.; Cuie, Y.; Fortin, G. R.; Winnik, F. M.; Maysinger, D. *J. Mol. Med.* **2005**, *83*, 377.

(28) Goodman, C. M.; McCusker, C. D.; Yilmaz, T.; Rotello, V. M. *Bioconjugate Chem.* **2004**, *15*, 897.

University and Scientific Research. We thank Dr. Nunzio Bottini (University of Southern California, Los Angeles, CA), Dr. Ana Miletic Sedy (Burnham Institute for Medical Research, La Jolla, CA), and Mr. Matthew H. Cato (Burnham Institute for Medical Research, La Jolla, CA) for helpful comments.

Supporting Information Available: Flow cytometry plots and statistical analyses. This material is available free of charge via the Internet at http://pubs.acs.org.

JA070245C